NMR structural analysis of incommensurate modulated systems with multiple active symmetry modes: A case study of deuterated bis-(4-chlorophenyl)-sulfone

C. Meinel, H. Zimmermann, and U. Haeberlen
Max–Planck–Institut für Medizinische Forschung, AG Molekülkristalle, Jahnstrasse 29, 69 120 Heidelberg, Germany

J. Etrillard
Groupe Matière Condensée et Matériaux, UMR au CNRS 6626, Université de Rennes 1, 35042 Rennes Cédex, France
(Received 16 July 1997)

We report single-crystal deuteron NMR measurements both in the normal (N) and the incommensurate (IC) phase of bis-(4-chlorophenyl)-sulfone (BCPS). From the quadrupole splitting data obtained in the N phase, the quadrupole coupling (QC) tensors of all deuterons in BCPS are derived. The central part of the paper is concerned with the analysis of the deuteron NMR frequency distributions observed in the IC phase as a function of the orientation of the applied magnetic field relative to the BCPS crystal. This analysis is carried out in terms of the amplitudes and phases of the rotational symmetry modes that contribute to the fundamental IC modulation wave in BCPS, i.e., directly in terms of the structural changes associated with the IC phase transition. Both a semiquantitative graphical, and a fully quantitative numerical approach are given. The former is used to identify particularly simple and therefore particularly informative crystal orientations. The latter uses as an input the deuteron QC tensors measured in the N phase. Quantitative and complete structural information about the rotational displacements that atoms experience in an N–IC phase transition is deduced from NMR spectra. Our results are in full agreement with corresponding data of an x-ray-diffraction study. We also report on measurements of the spin-lattice relaxation time T_1 across the deuteron NMR frequency distributions. The results are at variance with the established theory and this is traced back to the fact that multiple rotational modes are contributing to the IC modulation wave in BCPS. [S0163-1829(97)05342-3]

I. INTRODUCTION

The NMR spectra of single crystals of incommensurate (IC) systems display, instead of sharp resonances characteristic of normal (N) crystals, more or less broad, inhomogeneous frequency distributions. These frequency distributions result from the fact that nuclei in adjacent unit cells of an IC crystal are (slightly) displaced from their *average* positions and that, when viewed over the whole crystal, there is a continuum of such displacements. The displacements cause changes (often rotations) of the chemical shift and quadrupolar coupling tensors of the nuclei and these lead to variations of the chemical shifts ν and of the quadrupole satellite splittings $\Delta\nu_Q$ of the nuclear magnetic resonances.

Traditionally, the variation of these shifts and splittings is described by a ''coupling'' of the NMR frequency to the complex order parameter $\varrho = A\exp\{i\mathbf{k}_{IC}\cdot\mathbf{r}\}$ characterizing the IC phase of the crystal in the framework of the Landau theory of second-order phase transitions.[1] For simplicity we restrict ourselves here to systems with a one-dimensional IC modulation wave and to situations where the so-called plane-wave-limit approximation is applicable. A is the amplitude of the order parameter, $\mathbf{k}_{IC}$ the (frozen-in) incommensurate wave vector, and $\mathbf{r}$ is the position of the nucleus being considered. Depending on whether this nucleus occupies a *general* or *special* position of the average structure, the coupling of ν, respectively, $\Delta\nu_Q$, to the order parameter is usually assumed to be linear with a coupling constant c_1, or quadratic with a coupling constant c_2. For both the linear and quadratic cases, the shape of the resulting NMR frequency distribution can readily be calculated.[2] The parameters governing such a distribution are Ac_1 and Ac_2, respectively. These parameters provide little insight into what happens to the structure of the crystal at the N–IC phase transition, except that their temperature dependences reflect that of the order parameter and thus allows people to deduce the critical exponent β of the phase transition.

We will demonstrate in this paper that, provided that an IC phase can be studied by deuteron NMR, a direct and quantitative relation can be established between the observed NMR frequency distribution and the IC displacements of the deuterons. This is due to the fact that the quadrupole coupling tensor of a deuteron is, to an excellent approximation, rigidly connected to the bond by which the deuteron is connected to the rest of the rigid molecule, or to a rigid part of it such as a phenyl ring.

The displacements that atoms and rigid molecular entities experience in an N–IC phase transition constitute a frozen-in *normal mode* of the crystal in its N phase. Any displacement of a rigid entitiy can be described by a translation plus a rotation. Essentially, deuteron NMR senses only the rotation. Usually, it will be a small-angle rotation that can be represented by the components of a vector. These components need not be orthogonal. It is convenient to choose for these components the rotational symmetry modes contributing to the frozen-in normal mode. Each rotational symmetry mode is described by an amplitude α_{max}, a phase φ of the modulation function, and a rotation axis $\mathbf{R}$.

Crystals of bis-(4-chlorophenyl)-sulfone (BCPS), $SO_2(C_6H_4Cl)_2$, are monoclinic and possess twofold axes.[3,4]

Therefore, the symmetry modes can be classified according to whether they are invariant, or change sign under a C_2 rotation. The former are said to be of A or Λ_1, the latter of B or Λ_2 symmetry. Only modes of Λ_2 symmetry may contribute to the fundamental modulation wave of the frozen-in normal mode in BCPS.[5] By contrast, only modes of Λ_1 symmetry contribute to the second harmonic of the modulation wave. The complete description of the structural changes in a crystal during an N–IC phase transition is contained in the set of amplitudes and phases of the various symmetry modes. We point out, however, that these amplitudes and phases are not independent of each other. They are linked by the requirement that, together, they constitute a *normal mode* of the crystal. Therefore, the amplitudes will grow *unisono* on lowering the temperature while, ideally, the phases will remain unchanged.

For BCPS, such a complete description of the N–IC phase transition was achieved in an x-ray diffraction study and careful data analysis.[5] The aim of the present paper is, in principle, to reach the same goal by deuteron NMR. This general goal is, however, too ambitious. By the very nature of the deuteron NMR technique, we are limited to determining the amplitudes and phases of the *rotational* symmetry modes and, at least at the present time, we must restrict ourselves to the symmetry modes of the fundamental of the IC modulation wave, i.e., to the modes of Λ_2 symmetry. Our strategy will be to analyze the IC frequency distributions in a large number of deuteron NMR spectra recorded at different orientations of deuteron-enriched sample crystals relative to the applied field $\mathbf{B}_0$.

II. EXPERIMENTAL DETAILS

A. Samples

Fully deuterated bis-(4-chlorophenyl)-sulfone was prepared by oxidation of perdeuterated bis-(4-chlorophenyl)-sulfoxide with potassiumpermanganate.[6] The perdeuterosulfoxide was prepared by a Friedel-Crafts catalyzed reaction ($AlCl_3$) in which chlorobenzene-d_5 was reacted with $SOCl_2$.

For reasons which will become clear in Sec. III, we also made an effort to synthesize BCPS in which only the *ortho*-hydrogens (relative to chlorine) are deuterated. To this end 2.4.6-trideuterochlorobenzene was prepared out of 2.4.6-d_3-aniline. After the Friedel-Crafts reaction as above, NMR and mass spectroscopy showed some scrambling of the *ortho*-deuterons to the *meta* positions of the sulfoxide. The *ortho* positions were still deuterated to approximately 70%, while the *meta* positions were deuterated to about 30%. After oxidation, the deuterated BCPS was recrystallized from ethanol and sublimed twice.

Single crystals were grown by the Bridgeman method of both the fully deuterated and the 70% *ortho*, 30% *meta* deuterated BCPS. The (100) plane is an easy-cleavage plane of BCPS. This plane could easily be identified in our crystals and served as a welcome starting point for their final orientation by means of x rays.

From the oriented raw crystals, five samples I–V, fitting into standard 5 mm NMR tubes, were prepared for the deuteron NMR measurements. Samples I and II are fully deuterated, samples III–V are partially deuterated. The NMR probe is equipped with a goniometer that allows us to rotate the sample tube with the crystal inside about an axis perpendicular to $\mathbf{B}_0$. To specify crystal-fixed directions, such as the principal directions of quadrupole coupling tensors, but also the rotation axes of our sample crystals, we introduce a standard orthogonal axes system (SOS) with x_{SOS} parallel to the primitive crystal axis a, y_{SOS} parallel to the monoclinic axis b, and z_{SOS} parallel to the reciprocal-lattice axis c^*. In Table I we specify the directions of the rotation axes **s** of our sample crystals. In this table we also specify for each crystal a *reference direction* **d** and a *reference angle* α_{ref}. If, in the NMR goniometer, the rotation angle Ψ of the sample crystal equals the reference angle, the projection of **d** on the plane perpendicular to **s** is parallel to $\mathbf{B}_0$. Note that **s**, **d**, α_{ref}, and a rotation angle Ψ fully specify the direction of $\mathbf{B}_0$ in the crystal-fixed axes system SOS. Note also that the rotation axes of crystals I, III, and IV are approximately parallel to $z_{SOS}, -y_{SOS}$, and x_{SOS} and are thus along ''natural'' directions. The rotation axis of crystal V has been chosen to be perpendicular to the S–Cl direction of one of the wings of the BCPS molecule. This crystal can, therefore, be rotated into a position where $\mathbf{B}_0$ is parallel to the S–Cl direction which is special with regard to the incommensurate NMR frequency distributions, see Sec. V.

TABLE I. Directions of the rotation **s** and reference **d** axes and of the reference angles α_{ref} of the BCPS sample crystals I–V. Directions are specified by their polar angles θ and ϕ in the SOS. The last column indicates the deuteration of the respective sample crystals: fully (f) or selectively (s) in ortho positions.

	s		**d**		α_{ref}	Deuteration
Sample	θ_{rot}	ϕ_{rot}	θ_{ref}	ϕ_{ref}		
I	0.9°	325.0°	90°	90°	135.6°	f
II	90.5°	29.3°	90°	90°	103.0°	f
III	90.0°	270.0°	0°	0°	34.8°	s
IV	89.5°	1.0°	0°	0°	36.3°	s
V	90.1°	48.8°	0°	0°	-2.5°	s

B. NMR

All measurements we report were carried out on a home-built Fourier-transform spectrometer operating for deuterons at 72.13 MHz. The bulk of the data was acquired at $T = 100$ K. To reach this and lower temperatures, we used an Oxford Instruments helium-flow cryostat. The temperature was regulated with an ITC4 controller from the same company and was measured with a calibrated carbon glass sensor. The stability was better than ± 0.1 K.

Free induction decays (fids) were excited with $\pi/2$ pulses of duration 2.5μs. The fids were sampled with a dwell time of 1.5μs and Fourier transformed after discarding the first four data points which are spoiled by the pulse and its tail. The subtraction method of Speier[7] which cleans the fid from acoustic ringing effects, as well as Heuer's baseline cosine fitting (BCF) routine,[8] which reconstructs the discarded initial data points, were applied routinely. At $T = 100$ K, the spin-lattice relaxation time T_1 of the deuterons in BCPS varies, depending on the crystal orientation and on the spectral position in the IC frequency distribution, between 8 and 40

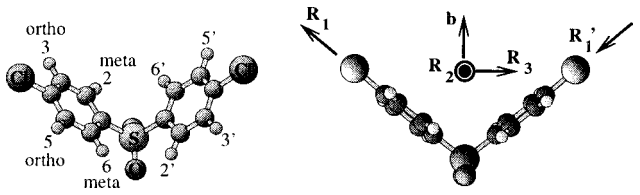

FIG. 1. The BCPS molecule, $SO_2(C_6H_4Cl)_2$, and our labeling of the deuterons. The two phenyl rings are related by a twofold axis parallel the crystal axis b. Right: the rotation axes $\mathbf{R}_1$, $\mathbf{R}_1'$, $\mathbf{R}_2$, and $\mathbf{R}_3$ of the rotational Λ_2 symmetry modes in the first harmonic of the IC modulation wave.

min. Because of these rather long relaxation times we restricted ourselves to recording just one fid for most of the spectra.

III. DEUTERON NMR SPECTRA AND QUADRUPOLE COUPLING (QC) TENSORS IN THE NORMAL PHASE OF BCPS

The normal phase of BCPS is monoclinic, space group $I2/a$, $Z=4$.[3,4] All four molecules in the unit cell are magnetically equivalent and the two wings of the molecule are related to each other by a twofold axis. Therefore, it is sufficient to specify the QC tensors of the deuterons of only one phenyl ring. We choose the ring of which the atomic positions are directly given in Table 8 of Ref. 3, and in Table I of Ref. 4. We also follow these references for labeling the deuterons, see the left part of Fig. 1.

Figure 2(a) shows a deuteron NMR spectrum of the fully deuterated sample I for $\Psi=140°$, recorded at ambiant temperature. It displays, as expected, eight doublets, i.e., one doublet from each of the eight deuteron positions in the molecule. The eight doublets come in four groups of two. This feature is quite general and not specific to the spectrum in Fig. 2(a). The doublets within each group arise from deuterons in opposite positions of the phenyl rings, e.g., from deuterons 3 and 6. These deuterons have nearly parallel bonds and therefore nearly equal QC tensors.

The almost but not perfectly coinciding resonances from deuterons in opposite positions complicate the interpretation

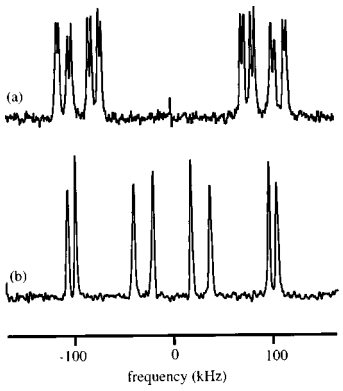

FIG. 2. Deuteron NMR spectra of BCPS at $T=290$ K. (a) Fully deuterated sample I, $\Psi=140°$. The doublets of all inequivalent hydrogen positions are resolved. All doublets appear in nearby pairs that arise from deuterons in opposing ortho/meta positions in the phenyl ring. (b) Sample V, selectively deuterated in the ortho positions, $\Psi=130°$. Only four doublets appear.

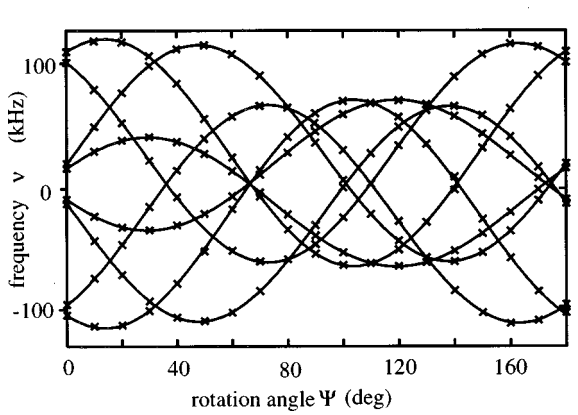

FIG. 3. Rotation pattern of NMR line positions of sample V at $T=155$ K. The curves display fittings to QC tensors.

of the frequency distributions in the IC phase of BCPS. This is the reason why we made the effort to synthesize BCPS with only the *ortho* hydrogen positions deuterated.

As stated in Sec. II A, we had only partial success. In the spectra of samples III–V the resonances of the *meta* deuterons are hardly visible or, at most, appear as mere shoulders of the resonances from the deuterons in the strongly deuterated opposite *ortho* positions, see Fig. 2(b). An undesired side effect of the specific deuteration is that the resonances are generally broader than in the fully deuterated samples. The reason for this effect is the much stronger deuteron-proton than deuteron-deuteron dipole-dipole interaction.

To get the necessary starting information for the interpretation of the frequency distributions in the IC phase of BCPS, we measured the deuteron QC tensors Q at $T=290$ K and at $T=155$ K, i.e., at 5 K above the N–IC phase transition. To this end we recorded from samples I and II (fully deuterated) at $T=290$ K sets of deuteron NMR spectra for increments of the rotation angle Ψ of 10°. Likewise, we recorded from samples III–V similar sets of spectra at $T=155$ K. The so-called rotation pattern of line positions for crystal V at T = 155 K is shown in Fig. 3. The data in this and the other rotation patterns were analyzed by a standard least-squares fitting procedure in terms of (traceless) QC tensors. In Table II we list the principal components Q_{XX}, Q_{YY}, Q_{ZZ}, the related quantities QCC$=\frac{2}{3}Q_{ZZ}$ (quadrupole coupling constant) and $\eta=(Q_{YY}-Q_{XX})/Q_{ZZ}$ (asymmetry parameter), and the principal directions $\mathbf{e}_X$, $\mathbf{e}_Y$, and $\mathbf{e}_Z$ of the deuteron QC tensors Q in BCPS, as measured at $T=290$ K. In Table III we give the same information for deuterons 3 and 5 at $T=155$ K.

Note that the QCC's found in BCPS are typical for aromatic deuterons.[10] They increase slightly on lowering T from 290 to 155 K which indicates that at 290 K there is some motional averaging due to thermally excited vibrations. The principal direction $\mathbf{e}_Z$ associated with the largest principal component, Q_{ZZ}, agrees for deuterons 3, 5, and 6 quite well with the corresponding C–D bond direction that follows from the neutron-diffraction data which we have, for convenience of the reader, also listed in Table II. For deuteron 2 the agreement is poor (deviation 6°). However, $\mathbf{e}_Z$ of deuteron 2 agrees quite well with the direction of the internuclear vector connecting the carbons C_2 and C_5 (deviation 1.6° respectively, 1.9°, depending on whether we take the

TABLE II. Deuteron QC tensors in BCPS at 290 K. Principal values and QCC's are given in units of kHz. The assignment of the signs to the principal components relies on the experience that QCC's of deuterons bound to carbons are positive (Ref. 9). The polar angles θ and ϕ of the principal directions $\mathbf{e}_X$, $\mathbf{e}_Y$, and $\mathbf{e}_Z$ are given with respect to the SOS axes system. For comparison, we give in the last two columns the C–D bond directions and the directions of the C_3–C_6 and C_2–C_5 internuclear vectors as determined by neutron and x-ray diffraction (Refs. 3 and 4).

Deuteron position[a]	Q_{XX} Q_{YY} Q_{ZZ}	θ	ϕ	QCC η	Bond directions from diffraction θ	ϕ
3	-136.9	107.2°	59.5°	177.9	52.4°[b]	341.9°
	-130.0	40.8°	128.4°	0.026	52.0°[c]	341.6°
	+266.8	54.4°	342.3°		52.4°[d]	341.4°
5	-137.5	111.4°	62.6°	178.1	21.8°[b]	83.1°
	-129.5	96.8°	155.3°	0.030	22.1°[c]	82.7°
	+267.1	22.5°	81.9°		22.6°[d]	78.7°
2	-135.7	112.6°	65.3°	176.7		
	-129.3	95.1°	157.5°	0.024		
	+265.0	23.2°	79.6°		24.1°[d]	94.3°
6	-138.1	112.5°	54.0°	176.8		
	-127.1	44.1°	118.7°	0.041		
	+265.2	54.4°	341.2°		52.8°[d]	340.7°

[a]Deuteron position according to Fig. 1.
[b]C–C direction as determined by neutron diffraction.
[c]C–C direction as determined by x-ray diffraction.
[d]C–D direction as determined by neutron diffraction.

x-ray or neutron-diffraction data for the C_2–C_5 direction). We think that the deviation of the C–D bond direction of deuteron 2 as determined by diffraction experiments from the C_2–C_5 direction (4.9°), also determined by diffraction, and from $\mathbf{e}_Z$ (6.0°) is indicative of an inaccuracy in the neutron-diffraction data.

Closing this section we would like to point out that it is very difficult to distinguish the QC tensors in opposite positions of the phenyl rings. As a matter of fact, we are not absolutely sure whether the assignment in Table II is correct or whether tensor 2 must be interchanged with tensor 5, and/or tensor 3 with tensor 6. Our assignment is based on the following (rather weak) arguments. First, the alternative assignments would make the increase of the QCC's from $T=290$ to 155 K larger than for the assignment we have chosen. We think that the smaller increase is more probable. Second, for the assignment chosen, the $\mathbf{e}_Z$'s of deuterons 3 and 6 agree better with the C–D bond directions following from the neutron-diffraction data than for the opposite choice. The same is true of the angle θ of the deuterons 5 and 2. As pointed out before, we do not trust the angle ϕ of the C–D bond direction of deuteron 2 (n diffraction). Fortunately, the uncertainty in the assignment of the 290 K QC tensors to deuterons 3 and 6, and to deuterons 2 and 5 is hardly of any relevance to the analysis of the observed frequency distributions in the incommensurate phase in BCPS to which we now turn.

TABLE III. QC tensors of the ortho-deuterons 3 and 5 in BCPS at $T=155$ K. Principal values and QCC's are given in units of kHz. The underlying quadrupole splitting data were collected from the selectively deuterated sample crystals III–V.

Deuteron position	Q_{XX} Q_{YY} Q_{ZZ}	θ	ϕ	QCC η
3	-141.2	104.7°	60.8°	179.1
	-127.6	41.0°	133.2°	0.051
	+268.7	52.8°	342.2°	
5	-138.0	106.6°	34.6°	180.8
	-133.1	106.9°	129.8°	0.014
	+271.1	24.0°	82.7°	

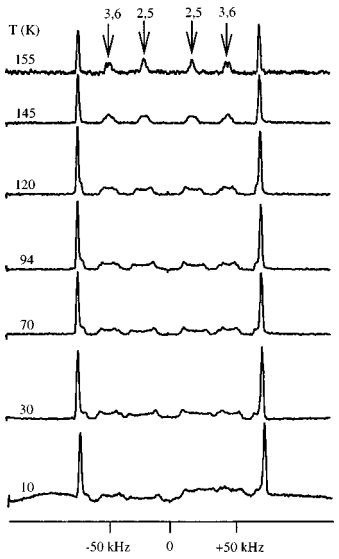

FIG. 4. Temperature evolution of deuteron NMR frequency distributions in the IC phase of BCPS in sample II, $\Psi=126°$. At $T=155$ K, all lines are narrow. Below $T_i=150$ K, most of the lines display a significant broadening which increases with decreasing temperature. The lineform is typical of crystals in a $1d$ IC phase. The outermost doublet remains accidentally narrow in this particular crystal orientation.

IV. TEMPERATURE DEPENDENCE OF DEUTERON NMR SPECTRA IN THE IC PHASE OF BCPS

In Fig. 4 we show the temperature evolution of the frequency distributions of the deuteron resonances in the IC phase of BCPS for the (fully deuterated) sample II, rotation angle $\Psi=126°$. In this series of spectra the innermost doublet stems, as indicated, from deuterons 2 and 5, the next one from deuterons 3 and 6, whereas the outermost doublet arises from the coinciding resonances of all deuterons in the ''other'' wing of the BCPS molecule. In the spectrum recorded at $T=155$ K the resonances of all deuterons are ''sharp,'' whereas at $T=145$ K the two inner doublets have developed into frequency distributions with distinct edges. For the deuterons of these doublets, the coupling of the order parameter to the quadrupole splitting $\Delta\nu_Q$ is linear to a very good approximation. The fact that the outermost doublet remains narrow is a consequence of the particular crystal orientation. On lowering the temperature to, ultimately, 10 K,

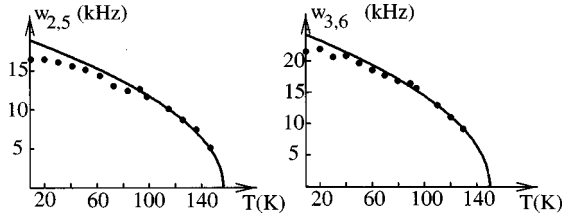

FIG. 5. Widths w between edges of the IC frequency distributions in the spectra of Fig. 4 vs T. Left: for deuterons 2 and 5; right: for deuterons 3 and 6. The curves are $w(T)=w_0(1-T/T_i)^{\beta}$ with $\beta=0.5$ and $T_i=150$ K.

the widths $w_{2,5}$ and $w_{3,6}$ between the edges of the frequency distributions increase gradually. This is displayed for the frequency distributions of deuterons 2 and 5, and 3 and 6 in Figs. 5(a) and 5(b). The curves in these figures represent the function $w(T)=w_0(1-T/T_i)^{\beta}$ with $T_i=150$ K and $\beta=0.5$. These functions obviously fit well the experimental data in the temperature range 90 K $<T<$ 150 K. This means that the N–IC phase transition in BCPS can be described by the Landau mean-field theory. The same conclusion was drawn from x-ray and neutron diffraction, Raman experiments, and ^{35}Cl NQR spectra of BCPS.[11–14] The finding of $\beta=0.5$ puts BCPS aside of numerous other IC systems including biphenyl, $C_{12}H_{10}$, and rubidium zinc chloride, Rb_2ZnCl_4, for which the nonclassical exponent $\beta=0.35$ has been determined[15] indicating that the appropriate Hamiltonian describing the phase transition is that of the three-dimensional XY model.[16]

V. ANALYSIS OF DEUTERON NMR FREQUENCY DISTRIBUTIONS FOR IC MODULATION WAVES WITH MULTIPLE SYMMETRY MODES

We will present two approaches for analyzing the shape and the width of the deuteron NMR frequency distributions in BCPS that are governed by the three Λ_2 symmetry modes of the fundamental IC modulation wave. The first approach is graphical and qualitative. It will help to understand, e.g., why and how the frequency distributions depend on the relative phases of the various symmetry modes and it will also help us to spot orientations of $\mathbf{B}_0$ that represent special and therefore most informative cases. The second approach is numerical and quantitative. It consists of simulating deuteron NMR spectra. It is based on the knowledge of the deuteron QC tensors Q in the normal phase of BCPS that we have measured and presented in Sec. III, and on the idea that Q follows rigidly any rotation of the rigid molecular entity to which the deuteron is bound covalently. For BCPS, this entity is the phenyl ring of one of the two wings. The x-ray work of Zuniga *et al.*[5] has established that this ring retains its shape in the IC phase, as expected, to an excellent approximation.

A. Graphical approach

The deuteron QC tensors Q in BCPS are nearly axially symmetric, i.e., $\eta \ll 1$, see Tables II and III. In this section we shall assume that $\eta=0$ and that the symmetry axis of Q coincides with the C–D bond direction. Then, the splitting

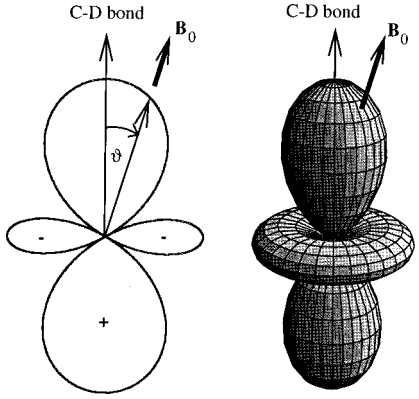

FIG. 6. Two- and three-dimensional graphical representations of a deuteron QC tensor, assumed to be axially symmetric, with the C–D bond as symmetry axis. In the text, such figures are called *tensors*. $\Delta\nu_Q$ is proportional to the distance from the center of the tensor to the point where $\mathbf{B}_0$ intersects the tensor surface. Apart from the QCC, $\Delta\nu_Q$ depends only on the angle ϑ. The sign of $\Delta\nu_Q$ is positive for $\vartheta<54.7°$ and negative for $54.7°<\vartheta\leq 90°$.

$$\Delta\nu_Q=\mathbf{b}_0\cdot\mathrm{Q}\cdot\mathbf{b}_0, \tag{1}$$

of a deuteron resonance varies, as a function of the angle ϑ between the bond and $\mathbf{B}_0$, according to

$$\Delta\nu_Q=\frac{3}{4}\,\mathrm{QCC}(3\cos^2\vartheta-1). \tag{2}$$

In Eq. (1), $\mathbf{b}_0=\mathbf{B}_0/|\mathbf{B}_0|$. Two- and three-dimensional representations of Eq. (2) are shown in Fig. 6. For brevity, a figure like that in Fig. 6(b) will be called a *tensor*. The length of the arrow in the direction of $\mathbf{B}_0$ from the center of the tensor to its surface is proportional to $\Delta\nu_Q$ of the respective deuteron.[17] Figure 7(a) shows the tensors of translationally equivalent deuterons in consecutive unit cells of a commensurate crystal. The C–D bonds are all parallel. When going from the N to the IC phase, the C–D bond directions experience rotations that are different in different unit cells. The QC tensors of the respective deuterons follow these rotations rigidly. Figure 7(b) shows schematically the tensors in the IC phase assuming, unrealistically but without consequences for NMR spectra, that the IC wavelength λ_{IC} is very much larger than the commensurate lattice period. The crosses in Fig. 7(a) and 7(b) mark the loci where $\mathbf{B}_0$ passes through the tensors. Relative to the tensors, the loci of these crosses are constant in the N phase, while they vary in the IC phase. For this reason, we see narrow lines in the N, and inhomogenously broadened lines in the IC phase. Now, let us look closer at the situation in the IC phase, change the point of view and move into an axes system in which the bond is fixed and in which, consequently, the direction of $\mathbf{B}_0$ moves as we proceed in the IC phase from one unit cell to the next. In this way, we get a mapping of the crosses from Fig. 7(b) onto one tensor. For an IC modulation wave with a single rotational symmetry mode, the map will be a (possibly curved) line. This is shown in Fig. 7(c). As shown in this figure, the length of the line will vary depending on the mean orientation of $\mathbf{B}_0$ relative to the bond (which can be controlled by the experimenter) and, as well, on the orientation of the axis $\mathbf{R}$ of the active rotational symmetry mode (which

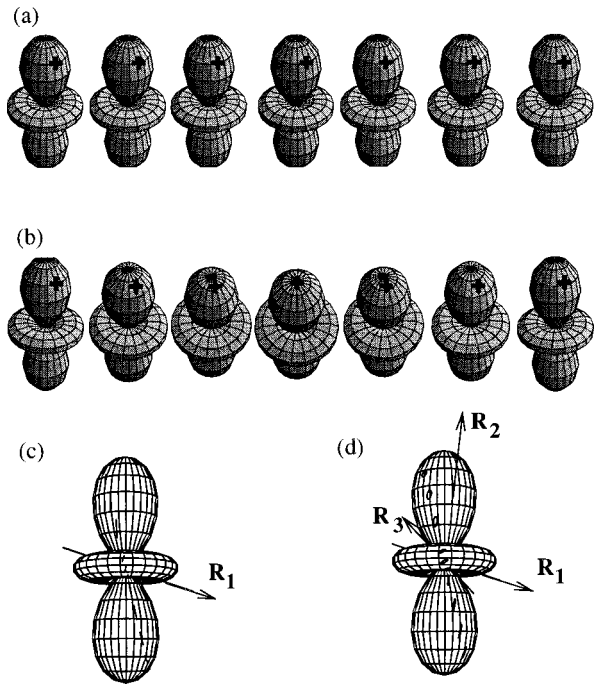

FIG. 7. Visualization of the origin and nature of IC frequency distributions. (a) N phase: the QC tensors are parallel in all unit cells. $\mathbf{B}_0$ intersects the tensor surfaces in the same point, indicated by a cross. $\Delta\nu_Q$ is the same for all deuterons, we see narrow lines in the spectrum. (b) IC phase: the QC tensors are no more parallel in adjacent unit cells, because the corresponding C–D bonds are not. Consequently, $\mathbf{B}_0$ intersects these tensors in different loci, indicated by crosses. $\Delta\nu_Q$ is different in all unit cells, we see frequency distributions in the spectra. (c) In an axes system, in which the C–D bond is fixed, $\mathbf{B_0}$ is modulated from cell to cell. We can map the occurring directions of $\mathbf{B}_0$ on one single tensor. For a single rotational symmetry mode, these directions are lying on a curved line. If the crystal is rotated, the line moves on the tensor surface, and its length and curvature change. (d) Same as (c) but multiple symmetry modes. The map of $\mathbf{B}_0$ is a Lissajous figure which changes size and shape depending on the crystal orientation. The rotation axes $\mathbf{R}_1$, $\mathbf{R}_2$, and $\mathbf{R}_3$ are realistic for BCPS. Note that the bond direction (the symmetry axis of the tensor), $\mathbf{R}_1$ and $\mathbf{R}_2$ are lying in a plane.

is a fixed crystal property). From Eq. (2) it follows that the mean latitude of the line, and the projection of the line onto a meridian of the tensor determines the width of the IC frequency distribution in the NMR spectrum. The *shape* of this distribution is determined by the density of crosses on the line. If the IC modulation wave is sinusoidal, the density has the shape of the histogram of a sinus function, that means, it has two edge singularities. If the mean orientation of $\mathbf{B}_0$ is far away from both the pole and the equator of the tensor, and if the line obtained by the mapping of the crosses is short, $\Delta\nu_Q$ will vary approximately linearly with ϑ along the line. In this approximation the histogram of the sinusoidal modulation function translates, with a rounding off of the singularities, directly into the shape of the frequency distribution in the NMR spectrum.

The ends of the lines in Fig. 7(c) correspond always to those deuterons whose bonds experience the extreme rotations during the N–IC phase transition. Thus, by measuring the orientation dependence of the edge singularities of the IC frequency distribution, we can determine the QC tensors of these deuterons, and, in so doing, the rotational amplitude of the IC modulation wave. This we have done, in essence, for biphenyl.[18] We will presently see that this procedure, appealing as it is, is limited to IC modulation waves consisting of only one single symmetry mode.

Let us now turn to IC modulation waves with multiple symmetry modes. To make the discussion realistic, we focus attention on deuteron 5 in BCPS. The axes $\mathbf{R}_i$ of the three rotational Λ_2 symmetry modes, which contribute to the fundamental IC modulatation wave in BCPS, are indicated in the right-hand part of Fig. 1. Relative to the bond of deuteron 5, these axes are situated as indicated in Fig. 7(d). The map of crosses from Fig. 7(b) onto the tensor is, in general, no longer a line but a kind of a Lissajous figure because the rotation angles

$$\begin{aligned}\alpha_1(\mathbf{r}_j) &= \alpha_{1,\max}\sin(\mathbf{k}_{\mathrm{IC}}\cdot\mathbf{r}_j+\varphi_1),\\ \alpha_2(\mathbf{r}_j) &= \alpha_{2,\max}\sin(\mathbf{k}_{\mathrm{IC}}\cdot\mathbf{r}_j+\varphi_2),\\ \alpha_3(\mathbf{r}_j) &= \alpha_{3,\max}\sin(\mathbf{k}_{\mathrm{IC}}\cdot\mathbf{r}_j+\varphi_3),\end{aligned} \tag{3}$$

associated with the three axes $\mathbf{R}_1,\mathbf{R}_2$, and $\mathbf{R}_3$ can have and *do* have in BCPS different phases φ_1,φ_2, and φ_3.[5] In Eq. (3), the index j labels the deuterons 5 in consecutive unit cells. In Fig. 7(d) we also show how the Lissajous figures change their shape as the mean orientation of $\mathbf{B}_0$ relative to the bond is changed.

The width of the NMR frequency distribution is again governed by the mean latitude of the Lissajous figure, and by the extension of the projection of the Lissajous figure onto a meridian of the tensor. Remarkably, the shape of the NMR frequency distribution is, irrespective of the shape of the Lissajous figure, the same as that for the single-symmetry-mode case. However, the NMR frequency distribution is no more a direct histogram of a modulation function. The three modulation functions in Eq. (3) lead to a certain density of crosses on the Lissajous figure. This density of crosses is projected onto a meridian of the tensor and it is this projection that we see in the NMR frequency distribution. This projection is equivalent to the histogram of a sinusoidal function, therefore the multiple-symmetry-mode and the single-symmetry-mode cases lead to the same shape of the NMR frequency distribution. However, there is one important difference between the two cases. When in the former case the mean orientation of $\mathbf{B}_0$ is changed, the edge singularities of the NMR frequency distribution arise, unlike in the latter case, from different deuterons in the crystal. This is the reason why the edge singularities do not arise from those deuterons whose bonds experience the extreme rotations during the N–IC phase transition. By following the orientational dependence of the quadrupole splittings $\Delta\nu_Q$ of the edge singularities, it is thus not possible to measure the QC tensor of any selected set of deuterons. That means, it is not possible to monitor in this way the rotational displacements of any set of deuterons during the N–IC phase transition. This fact complicates the analysis of IC frequency distributions resulting from multiple symmetry modes and also affects, as we shall see in Sec. VI, the variation of T_1 across the frequency distribution.

Still, from Fig. 7(d) it is intuitively clear that there are special orientations of $\mathbf{B}_0$ which simplify the situation. One of them is obtained when the mean orientation of $\mathbf{B}_0$ coincides with any of the axes $\mathbf{R}_i$. In such a case, the respective symmetry mode will not contribute to the NMR frequency distribution. Another special case is obtained when one of the symmetry modes does not contribute to the extension of the Lissajous figure along a meridian of the tensor. This happens whenever the bond direction, a rotation axis $\mathbf{R}_i$, and the mean orientation of $\mathbf{B}_0$ are lying in one plane. This special case may arise simultaneously for two rotation axes $\mathbf{R}_i$ and $\mathbf{R}_j$, namely, when the bond direction, $\mathbf{R}_i$ as well as $\mathbf{R}_j$ are all lying in a plane. If, in such a case, we move $\mathbf{B}_0$ into the same plane, both symmetry modes i and j will not contribute to the width of the NMR frequency distribution. A look at the right-hand part of Fig. 1 will convince the reader that the rotation axes $\mathbf{R}_1$ and $\mathbf{R}_2$, and the bond directions of all (unprimed) deuterons of the BCPS molecule are almost lying in one plane. This gives us the chance to record deuteron NMR frequency distributions from BCPS whose widths are almost exclusively due to the third rotational symmetry mode and thus allow a direct determination of $\alpha_{3,\max}$ in Eq. (3). This doubly special situation we have exploited in our experiments on BCPS, see Sec. V C.

B. Numerical simulation of IC frequency distributions

The ingredients of the simulations are as stated in the introductory paragraph of this section. In addition, we exploit the fact that, in the IC phase of the crystal, the set of numbers $\mathbf{k}_{\mathrm{IC}}\cdot\mathbf{r}_j$ *modulo* 2π is dense in the interval $0-2\pi$ and that the density is constant. For our simulations we subdivide the interval $0-2\pi$ into a large number K of equal steps, e.g., $K=100$. The QC tensor $\mathsf{Q}^{(k)}$ of a particular deuteron in the molecule corresponding to the kth step will be

$$\mathsf{Q}^{(k)}=D_1(\alpha_1^{(k)})\cdot D_2(\alpha_2^{(k)})\cdot D_3(\alpha_3^{(k)})\cdot \mathsf{Q}_N \times D_3^{-1}(\alpha_3^{(k)})\cdot D_2^{-1}(\alpha_2^{(k)})\cdot D_1^{-1}(\alpha_1^{(k)}), \qquad (4)$$

where Q_N is the known QC tensor of this deuteron in the normal phase of the crystal and

$$\alpha_n^{(k)}=\alpha_{n,\max}\cdot\sin\left(2\pi\cdot\frac{k}{K}+\varphi_n\right). \qquad (5)$$

The $D_n(\alpha_n^{(k)})$ in Eq. (4) are the rotation matrices corresponding to the various rotational Λ_2 symmetry modes of the IC modulation wave. The quadrupole splitting of the NMR of this deuteron will be

$$\Delta\nu_Q^{(k)}=\mathbf{b}_0\cdot\mathsf{Q}^{(k)}\cdot\mathbf{b}_0. \qquad (6)$$

Equation (4) implies a certain order in which the rotations are carried out. This order is unknown. Fortunately, it is irrelevant because all the $\alpha_n^{(k)}$ are small, see below.

By folding the kth stick spectrum by a Gaussian of appropriate width and summing over k, we get the IC frequency distribution of this particular deuteron for the chosen orientation of $\mathbf{B}_0$. Superimposing the frequency distributions of all four *ortho*, respectively, all eight *distinct* deuterons of the BCPS molecule yields the spectrum that can be compared with the experimental one for the same orientation of $\mathbf{B}_0$.

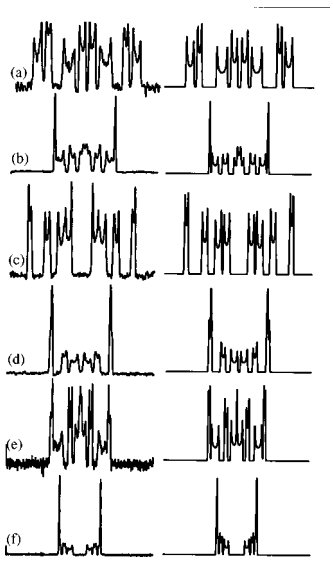

FIG. 8. Left: deuteron spectra of crystals of BCPS in different orientations, $T=100$ K. (a)–(d) crystal V, $\Psi=40°$, 100°, 10°, 115°, total spectral width 333 kHz; (e),(f) crystal II, $\Psi=60°$, 130°, total spectral width 500 kHz. Right: simulations for the same crystal orientations and $\alpha_{1,\max}$, $\alpha_{2,\max}$, $\alpha_{3,\max}$, $\varphi_2-\varphi_1$, $\varphi_3-\varphi_1$ as determined in Sec. V.

C. Application to BCPS

Because the NMR frequency distribution is independent of the phase of the modulation wave, which we may identify with φ_1 without loss of generality, there remain five parameters that enter the simulations. These parameters are $\alpha_{1,\max},\alpha_{2,\max},\alpha_{3,\max}$, and $\varphi_2-\varphi_1,\varphi_3-\varphi_1$. We wish to determine these parameters from a comparison of experimental with simulated spectra. It is clear from the outset that it is not sufficient to compare a single experimental spectrum with simulations for the same orientation of $\mathbf{B}_0$ that are carried out with different parameters.

Thus, from all sample crystals I–V, we recorded, varying the rotation angle Ψ, a total of 52 deuteron NMR spectra at $T=100$ K. Six of these spectra are reproduced in Fig. 8. They document how strongly the overall appearance of the spectra, and as well, the IC frequency distributions change when the orientation of $\mathbf{B}_0$ relative to the crystal is changed. Obviously, these spectra contain a rich amount of information. However, it is a formidable task to extract from them this information in the form of the desired parameters $\alpha_{1,\max}\ldots,\varphi_3-\varphi_1$. Therefore, we begin the analysis with the special cases discussed in Sec. V A.

As mentioned in Sec. II A, sample V allows us to rotate the crystal such that $\mathbf{B}_0$ is parallel to the S–Cl direction of the unprimed wing of the BCPS molecule and thus along the axis $\mathbf{R}_1$. For this situation, the rotational symmetry mode 1 does not contribute to the width of the IC frequency distributions of the unprimed deuterons. Neither contributes the rotational symmetry mode 2, because in this doubly special situation $\mathbf{R}_2$ is, in addition, (almost) in the plane that is spanned by $\mathbf{B}_0$ and any of the C–D bonds in this wing.

The experimental spectrum for this crystal orientation is shown in line (a) of Fig. 9. The resonances marked by the arrows arise from *all* unprimed deuterons because the angle ϑ between $\mathbf{B}_0$ and the bond of each of these deuterons is the

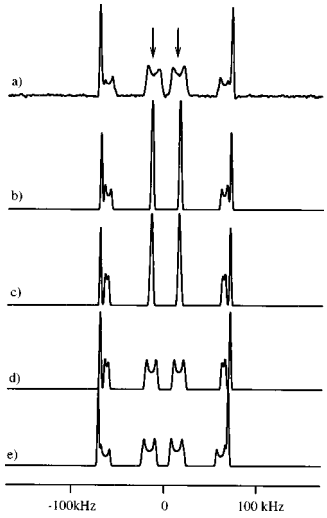

FIG. 9. (a) Deuteron spectrum of crystal V, $\Psi = 106°$, $T = 100$ K. $\mathbf{B}_0$ is almost parallel to the S–Cl direction of one phenyl ring. (b)–(e) simulations with different parameter sets. (b) $\alpha_{1,\max} = 3.2°$, $\alpha_{2,\max} = \alpha_{3,\max} = 0°$; (c) $\alpha_{2,\max} = 3.0°$, $\alpha_{1,\max} = \alpha_{3,\max} = 0°$; (d) $\alpha_{3,\max} = 3.2°$, $\alpha_{1,\max} = \alpha_{2,\max} = 0°$. The phases $\varphi_2 - \varphi_1$ and $\varphi_3 - \varphi_1$ are irrelevant in simulations (b)-(d). (e) $\alpha_{1,\max} = \alpha_{3,\max} = 3.2°$, $\alpha_{2,\max} = 3.0°$, $\varphi_2 - \varphi_1 = 65°$, $\varphi_3 - \varphi_1 = 300°$.

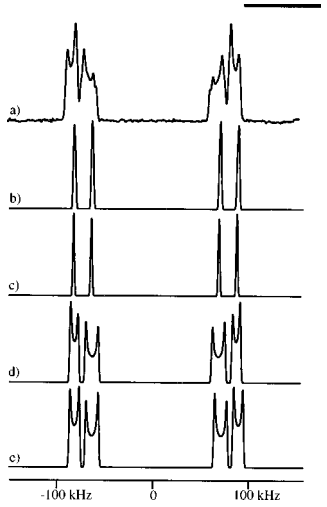

FIG. 10. (a) Deuteron spectrum of crystal III, $\Psi = 10°$, $T = 100$ K. $\mathbf{B}_0$ is *in* the monoclinic plane and almost parallel to $\mathbf{R}_2$. (b)–(e) simulations with different parameter sets. (b) $\alpha_{1,\max} = 3.2°$, $\alpha_{2,\max} = \alpha_{3,\max} = 0°$; (c) $\alpha_{2,\max} = 3.0°$, $\alpha_{1,\max} = \alpha_{3,\max} = 0°$; (d) $\alpha_{3,\max} = 3.2°$, $\alpha_{1,\max} = \alpha_{2,\max} = 0°$. The phases $\varphi_2 - \varphi_1$ and $\varphi_3 - \varphi_1$ are irrelevant in simulations (b)-(d). (e) $\alpha_{1,\max} = \alpha_{3,\max} = 3.2°$, $\alpha_{2,\max} = 3.0°$, $\varphi_2 - \varphi_1 = 65°$, $\varphi_3 - \varphi_1 = 300°$. The shoulder on the inner flank of the inner of the two frequency distributions in (a) indicates a slight deviation of $\mathbf{B}_0$ from the monoclinic plane.

same for $\mathbf{B}_0 \| \text{S–Cl}$, namely 60°. The resonances in Fig. 9 with the larger quadrupole splittings arise from the deuterons of the other wing. For the moment, we disregard them.

Having been biased from our experience with biphenyl where a rotation about the long axis of the molecule constitutes the only symmetry mode of the IC modulation wave, we were surprised to see in BCPS a broad frequency distribution for $\mathbf{B}_0 \| \mathbf{R}_1$, i.e., when IC rotations about the S–Cl direction cannot cause a spread of the deuteron resonances. The spectrum in Fig. 9(a) provides, therefore, direct and immediate evidence that other symmetry modes of the IC modulation wave must exist in BCPS. The simulated spectrum in Fig. 9(b), which was calculated under the assumption that the symmetry mode 1 is the only active one, proves this point: This spectrum shows no IC spread of the inner resonances. As discussed above, we expect that for $\mathbf{B}_0 \| \text{S–Cl}$ the symmetry mode 2 as well does not contribute to the width of the IC frequency distribution. This is demonstrated by the simulation in Fig. 9(c) (the simulation parameters are listed in the figure caption). In line (d) of Fig. 9 we display a simulation that was calculated under the assumption that only the rotational symmetry mode 3 is active. Under this assumption, we do get a spread of the resonances and the width of the IC frequency distribution depends only on $\alpha_{3,\max}$. By adjusting $\alpha_{3,\max}$ in the simulations such as to obtain the best match between the (inner) resonances of the simulation [line (d)] and those of the experimental spectrum [line (a)], we conclude that $\alpha_{3,\max}$ must be $3.2° \pm 0.2°$. We stress that this number applies to $T = 100$ K. Anticipating the determination of the other amplitudes $\alpha_{n,\max}$ and that of the relative phases $\varphi_n - \varphi_m$, we show in line (e) of Fig. 9 the simulated spectrum calculated with the final amplitudes and the final relative phases. As can be seen, the inner resonances hardly change when going from line (d) to line (e), however, the outer resonances in line (e) also agree, unlike those in line (d), remarkably well with those in the experimental spectrum.

The foregoing discussion applies also to the other doubly special case, namely when $\mathbf{B}_0$ is parallel to $\mathbf{R}_2$. Unlike $\mathbf{R}_1$, however, $\mathbf{R}_2$ is lying in the monoclinic plane of the crystal. Therefore, the resonances of pairs of symmetry-related deuterons 5 and 5', etc., on the two wings of the BCPS molecule must coincide for $\mathbf{B}_0 \| \mathbf{R}_2$. For an exact hexagon-symmetry of the aromatic rings even the resonances of *all* deuterons should coincide. To avoid this only approximately fulfilled special situation, we recorded a spectrum with $\mathbf{B}_0$ lying in the monoclinic plane, but (nominally) 4.3° off $\mathbf{R}_2$ (away from the $-c^*$ direction). The deviation of 4.3° is small enough, on the one hand, for the consequences of the doubly special case $\mathbf{B}_0 \| \mathbf{R}_2$ to apply at least approximately, and, on the other hand, it is large enough to separate the resonances of deuterons 5 and 5' from those of deuterons 3 and 3'. This spectrum is shown in line (a) of Fig. 10. Lines (b)–(e) display analogous simulations as in Fig. 9. The new feature in Fig. 10 is that both pairs of resonances behave alike whereas they behaved differently in Fig. 9. The quantitative conclusion from the experimental spectrum in line (a) of Fig. 10 and from the simulations in lines (d) and (e) is the confirmation that $\alpha_{3,\max}$ must be $3.2° \pm 0.2°$ at $T = 100$ K.

Unfortunately, there are no *doubly special* orientations of $\mathbf{B}_0$ that would allow a separate determination of $\alpha_{1,\max}$ and $\alpha_{2,\max}$, and of $\varphi_2 - \varphi_1$ and $\varphi_3 - \varphi_1$. The reason is that neither $\mathbf{R}_1$ nor $\mathbf{R}_2$ are lying in the plane spanned by any of the C–D bonds and $\mathbf{R}_3$. Therefore, in our further analysis of the experimental spectra, we had to go the hard road which means testing numerous simulations with different sets of parameter values. The criterium for *success* was a match of the width of all IC frequency distributions in the experimental and simulated spectra for all 52 different orientations of $\mathbf{B}_0$. How sensitively these widths depend on the relative phases $\varphi_2 - \varphi_1$ and $\varphi_3 - \varphi_1$ is illustrated in Fig. 11. In the

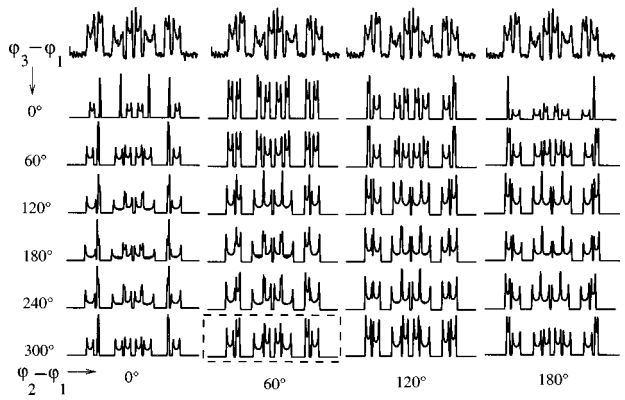

FIG. 11. Top line: Four replications of the deuteron spectrum of crystal V, $\Psi = 40°$. Below: a matrix of simulations for different combinations of relative phases $\varphi_2 - \varphi_1$ and $\varphi_3 - \varphi_1$ and fixed amplitudes $\alpha_{1,\max} = \alpha_{3,\max} = 3.2°$, $\alpha_{2,\max} = 3.0°$. The best match of simulation and experiment is achieved with $\varphi_2 - \varphi_1 = 60°$ and $\varphi_3 - \varphi_1 = 300°$ (framed simulation).

top row of this figure we have reproduced four times the spectrum (a) from Fig. 8. Below this experimental spectrum we show a matrix of 24 simulated spectra, calculated for different values of $\varphi_2 - \varphi_1$ and $\varphi_3 - \varphi_1$. Except for the simulation marked by a frame, a single glance is sufficient to rule out the respective combination of phases. On the other hand, in the framed simulated spectrum, the widths of all four IC frequency distributions match the corresponding widths in the experimental spectrum quite well. That means, the parameter set used for this simulation, is a candidate for *success*. A search on a finer grid revealed that the best match is obtained for

$$\alpha_{1,\max} = 3.2° \pm 0.2°, \quad \varphi_2 - \varphi_1 = 65° \pm 10°,$$

$$\alpha_{2,\max} = 3.0° \pm 0.2°, \quad \varphi_3 - \varphi_1 = 300° \pm 10°,$$

$$\alpha_{3,\max} = 3.2° \pm 0.2°.$$

This set of parameters led to the simulated spectra in Fig. 8 that match well the corresponding experimental ones. As a matter of fact, all of the 52 spectra recorded at $T = 100$ K can be reproduced reasonably well by simulations with the above set of parameters. We may thus claim that this set of amplitudes and phases of the three rotational symmetry modes describes the rotational part of the fundamental IC modulation wave in BCPS at $T = 100$ K.

VI. DEUTERON SPIN-LATTICE RELAXATION

In sample V at the rotation angles $\Psi = 10°$ and $\Psi = 40°$, we measured, using the saturation-recovery method, at four different temperatures 100 K $\leqslant T_k \leqslant$ 145 K the deuteron spin lattice relaxation time across the IC frequency distributions. A C^{++} program was written that takes as input directly the Fourier spectra for different relaxation delays and performs a least-squares fitting of the recovery curves to exponentials for each of the discrete frequencies in the spectrum. Figure 12 shows the result for $T = 100$ K in both crystal orientations. We recognize that T_1 varies across the IC frequency distributions, depends on the crystal orientation relative to $\mathbf{B}_0$ and also on the site of the deuteron in the BCPS molecule. The

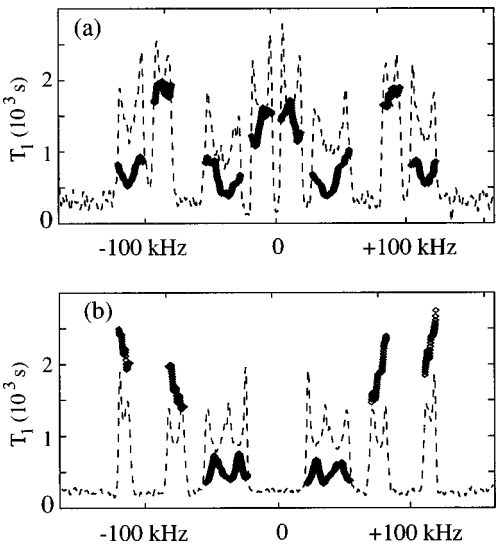

FIG. 12. Variation of deuteron spin-lattice relaxation time T_1 across the spectrum in crystal V at (a) $\Psi = 40°$ and (b) $\Psi = 10°$, $T = 100$ K. Spectra are displayed by dashed lines. Note that the two innermost doublets in (b) have a frequency dependence of T_1 opposite to that predicted by the classical theory: the edge singularities relax more rapidly than the centers of the frequency distributions. The two outermost doublets in (b) show an almost linear increase of T_1 across the frequency distribution.

smallest T_1's encountered are 500 s, the largest 2300 s. Similarly to the case of ^{35}Cl[14], the ratios $T_{1\max}/T_{1\min}$ within the deuteron frequency distributions do not deviate *very* much from unity. This is at variance with the classical theory of Žumer and Blinc.[19] This theory predicts that the edge singularities of the IC frequency distributions should not be sensitive to so-called phasons, and therefore should exhibit longer (even very much longer) relaxation times than the centers of the frequency distributions which *are* sensitive to phasons.

This predicition fails even qualitatively for BCPS: For both inner pairs of resonances in Fig. 12(b), it is the *center* of the distribution, rather than the edge singularities, which has the longer relaxation times. That shows right away that any attempt to deduce the size of a phason gap from the T_1 ratio of the center and the singularities of the frequency distribution is bound to fail. After all, the gap of the phason cannot be larger than that of the amplitudon. As regards the outer pairs of resonances, the relaxation time appears to increase monotonically across the frequency distribution. That means, the edge singularities relax with a different rate. This stresses once more that for IC modulation waves with multiple symmetry modes it is not possible to assign the nuclei belonging to the edge singularities in the spectrum to any maxima or minima of the modulation wave.

Finally, we may compare, after proper scaling, the deuteron relaxation times with the ^{35}Cl relaxation time measured in BCPS.[14] At $T = 100$ K, Mikac *et al.* found $T_1(^{35}\mathrm{Cl}) \approx 7$ ms (average over the frequency distribution). The proper scaling factor S is the square of the ratio of the strengths of the quadrupole interactions, i.e.,

$$S = \left(\frac{\mathrm{QCC}(^{35}Cl)}{\mathrm{QCC}(^{2}H)} \right)^2 \approx \left(\frac{35\ \mathrm{MHz}}{178\ \mathrm{kHz}} \right)^2 \approx 4 \times 10^4. \qquad (7)$$

Assuming that the dynamics of the ^{35}Cl and ^{2}H QC tensors is the same, we thus arrive at the estimate

$$T_{1,\text{estimate}} = S \cdot T_1(^{35}\text{Cl}) \approx 280 \text{ s} \tag{8}$$

for the deuteron relaxation time at $T = 100$ K. This estimate compares favorably with our direct experimental result and indicates that the dynamics of the ^{35}Cl and ^{2}H QC tensors is indeed essentially the same.

VII. DISCUSSION AND OUTLOOK

The central result of this paper is the deuteron NMR determination of the amplitudes and relative phases of the three rotational symmetry modes of the fundamental IC modulation wave in BCPS. This was achieved by linking the IC frequency distributions with the spread of the C–D bond directions.

We recall that this determination was done at $T = 100$ K. From an analysis of x-ray diffraction patterns, Zuniga *et al.*[5] determined in 1993 the same set of parameters at $T = 90$ K. Their result is (error limits are not given)

$$\alpha_{1,\max} = 3.5°, \quad \varphi_2 - \varphi_1 = 72°,$$
$$\alpha_{2,\max} = 3.3°, \quad \varphi_3 - \varphi_1 = 302°,$$
$$\alpha_{3,\max} = 3.5°.$$

It is highly satisfying that both the x-ray and the deuteron NMR methods lead to the same result within our error limits. Of course, our work was done with full knowledge of the paper of Zuniga *et al*. Therefore, one might suspect that our work is not independent of theirs. This is indeeed the case, however, only in so far as we learned what the allowed rotational symmetry modes of the fundamental IC modulation wave are in BCPS. Our determination of the parameter set $\alpha_{1,\max} \cdots \varphi_3 - \varphi_1$ is independent. We have documented this in some detail for $\alpha_{3,\max}$. After having determined $\alpha_{3,\max}$, we were aided, somewhat, by Zuniga *et al.*'s values of $\alpha_{2,\max}$ and $\alpha_{1,\max}$. Nevertheless, there can be no doubt that our set of deuteron NMR spectra in its entirety does contain the full information about all parameters $\alpha_{1,\max}, \ldots, \varphi_3 - \varphi_1$.

So far, we focused attention exclusively on the fundamental IC modulation wave. Correspondingly, we focused attention on the *widths* of the IC frequency distributions. On the other hand, Zuniga *et al*. report also about a finite second harmonic. The contributing modes are of symmetry Λ_1.

While the *shape* of an IC frequency distribution does not depend on whether there are one or several active symmetry modes of an IC modulation wave, it does depend on the presence or absence of harmonics. The experimental spectrum in Fig. 13(a) shows some conspicuous deviations from the familiar shape. They are marked by arrows. We wondered whether they arise from the second harmonic. To find out we again returned to simulations.

Our simulation program can easily incorporate harmonics. All that is needed is to supplement Eqs. (3) by the harmonic terms. Including the second harmonic, these equations now read

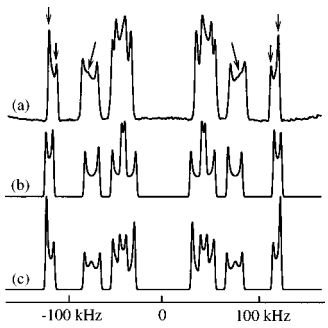

FIG. 13. Influence of the second harmonic of the IC modulation wave on deuteron NMR spectrum in crystal V, $\Psi = 20°$. (a) Spectrum at $T = 100$ K; the arrows point to features of IC frequency distributions (hump in the center, one horn is much larger than the other) that are inconsistent with a purely sinusoidal modulation wave. (b) Simulation including only the first harmonic with parameters as deduced in Sec. V. (c) Simulation including the first harmonic as in (b) and additionally the second harmonic with $\alpha'_{1,\max} = 0.6°$, $\alpha'_{2,\max} = \alpha'_{y,\max} = 0.7°$, $\varphi'_1 = 280°$, $\varphi'_2 = 223°$, and $\varphi'_y = 144°$. Apart from φ'_y, these values are those from Zuniga *et al.* Zuniga's value for φ'_y is $36° = 180° - 144°$.

$$\alpha_n(\mathbf{r}_j) = \alpha_{n,\max} \cdot \sin(\mathbf{k}_{\text{IC}} \cdot \mathbf{r}_j + \varphi_n) + \alpha'_{n,\max} \cdot \sin(2\mathbf{k}_{\text{IC}} \cdot \mathbf{r}_j + \varphi'_n).$$

The $\alpha'_{n,\max}$ and φ'_n are the amplitudes and phases of the rotational symmetry modes of the second harmonic. Note that $\mathbf{R}_3$ does not contribute in the second harmonic, whereas $\mathbf{R}_y$ does contribute in the second, but not in the first harmonic.[5] In parts (b) and (c) of Fig. 13, we show two simulations. The first was calculated as before, i.e., taking into account only the fundamental wave, while the latter includes the second harmonic with the amplitudes $\alpha'_{n,\max}$ and phases φ'_n as given in Ref. 5, see, however, figure caption. This simulation exhibits all the conspicuous features present in the experimental spectrum and thus suggests that these features indeed arise from the second harmonic. Unfortunately, the features in the deuteron NMR spectra originating in the second-harmonic IC wave are too weak and are seen in too few of the experimental spectra to warrant an attempt of determining the amplitudes $\alpha'_{n,\max}$ and phases φ'_n by the same deuteron NMR strategy that was successful for the fundamental modulation wave. By lowering the temperature to a value far below 100 K, the second harmonic will become stronger and, as well, the respective features in the deuteron NMR spectra will also become more pronounced. This will improve the chances to determine the structural parameters of the second harmonic by deuteron NMR. However, preliminary neutron-diffraction experiments show that at $T = 10$ K the distortion of the IC modulation wave comprises at least five harmonics, all of which will affect the deuteron NMR spectra.

ACKNOWLEDGMENTS

We greatly enjoyed and profited from both oral and electronic mail discussions with B. Toudic, R. Blinc, and, in particular, J. M. Pérez-Mato.

[1] R. Blinc, P. Prelovsek, V. Rutar, J. Seliger, and S. Žumer, in *Incommensurate Phases in Dielectrics*, edited by R. Blinc and A. P. Levanyuk, Modern Problems in Condensed Matter Sciences Vol. 1 (North-Holland, Amsterdam, 1986).
[2] R. Blinc, Phys. Rep. **79**, 331 (1981).
[3] J. G. Sime and S. C. Abrahams, Acta Crystallogr. **13**, 1 (1960).
[4] G. E. Bacon and N. A. Curry, Acta Crystallogr., **13**, 10 (1960).
[5] F. J. Zuniga, J. M. Pérez-Mato, and T. Breczewski, Acta Crystallogr., Sect. B: Struct. Sci. **49**, 1060 (1993).
[6] C. W. N. Cumper, J. F. Read, and A. I. Vogel, J. Chem. Soc. 5860 (1965).
[7] P. Speier, G. Prigl, H. Zimmermann, U. Haeberlen, E. Zaborowski, and S. Vega, Appl. Magn. Reson. **9**, 81 (1995).
[8] A. Heuer and U. Haeberlen, J. Magn. Reson. **85**, 79 (1989).
[9] C. Müller, S. Idziak, N. Pislewski, and U. Haeberlen, J. Magn. Reson. **47**, 227 (1982).
[10] R. G. Barnes, in *Advances in Nuclear Quadrupole Resonance* edited by J. A. S. Smith (Heyden, London, 1974), Vol. 1, p. 335, Table II.
[11] H. Kasano, T. Koshiba, H. Kasatani, and H. Terauchi, J. Phys. Soc. Jpn. **59**, 408 (1990).
[12] J. Etrillard, J. Even, M. Sougoti, P. Launois, S. Longeville, and B. Toudic, Solid State Commun. **87**, 47 (1993).
[13] K. Ishii, H. Nakayama, T. Sakato, and H. Kano, J. Phys. Soc. Jpn. **61**, 2317 (1992).
[14] U. Mikac, T. Apih, M. Koren, J. Dolinsek, J. Seliger, J. Slak, and R. Blinc, Phys. Rev. B **54**, 9141 (1996).
[15] F. Decker, U. Häcker, K.-P. Holzer, P. Mischo, J. Petersson, and D. Michel, Ferroelectrics (to be published).
[16] A. D. Bruce and R. A. Cowley, J. Phys. C **11**, 3577 (1978).
[17] J. A. Weil, T. Buch, and J. E. Clapp, in *Advances in Magnetic Resonance*, edited by J. S. Waugh (Academic, New York, 1973), Vol. 6, p. 183.
[18] L. von Laue, F. Ermark, A. Gölzhäuser, U. Haeberlen, and U. Häcker, J. Phys. C **8**, 3977 (1996).
[19] S. Žumer and R. Blinc, J. Phys. C **14**, 465 (1981).